

Physical conditions that lead to the detection of the pair annihilation line in the BOAT GRB221009A

ASAF PE'ER¹ AND BING ZHANG^{2,3}

¹*Bar-Ilan University, Ramat-Gan 5290002, Israel*

²*The Nevada Center for Astrophysics, University of Nevada, Las Vegas, NV 89154, USA*

³*Department of Physics and Astronomy, University of Nevada, Las Vegas, NV 89154, USA*

ABSTRACT

The brightest of all time (BOAT) GRB221009A show evidence for a narrow, evolving MeV emission line. Here, we show that this line can be explained as due to pair annihilation in the prompt emission region, and that its temporal evolution is naturally explained as the high-latitude emission (emission from higher angles from the line of sight) after prompt emission is over. We consider both the high and low optical depth for pair production regimes, and find acceptable solutions, with the GRB Lorentz factor $\Gamma \approx 600$ and the emission radius $r \gtrsim 10^{16.5}$ cm. We discuss the conditions for the appearance of such a line, and show that a unique combination of high luminosity and Lorentz factor that is in a fairly narrow range are required for the line detection. This explains why such an annihilation line is rarely observed in GRBs.

Keywords: Relativistic jets — High energy astrophysics — Gamma-ray bursts — Theoretical models

1. INTRODUCTION

Gamma-ray bursts (GRBs) are the most extreme explosions in the universe, releasing, in many cases more than $10^{52} - 10^{53}$ ergs within a few seconds. This energy release occurs in a very compact region, comparable to the core of a collapsing, massive star, namely $10^7 - 10^8$ cm (see Mészáros 2006; Pe'er 2015; Kumar & Zhang 2015; Zhang 2018; Mészáros 2019; Bošnjak et al. 2022, for a few recent reviews). Observations of very energetic photons, in the MeV-GeV (and recently, TeV) range, thus imply that the explosion energy must first be converted to kinetic energy in the form of relativistic jet before dissipation causes the release of the gamma-ray signal. Jet Lorentz factor of $\Gamma \geq 100$ is typically needed to solve the compactness problem (Krolik & Pier 1991; Woods & Loeb 1995; Lithwick & Sari 2001); but see Dereli-Bégué et al. (2022). Explosion energy conversion to kinetic energy can be mediated either by photons (the well known "fireball" model; Cavallo & Rees 1978; Shemi & Piran 1990; Rees & Meszaros 1992; Meszaros & Rees 1993; Rees & Meszaros 1994) or by strong magnetic fields (Drenkhahn 2002; Drenkhahn & Spruit 2002; Mészáros & Rees 1997; Zhang & Pe'er 2009; Zhang & Yan 2011). In either scenario, a large number of e^\pm -pairs is expected to be created, by interaction of energetic photons having (comoving) energies exceeding the threshold energy of 0.511 MeV.

Although the creation of a large number of pairs was predicted a long time ago (Pe'er & Waxman 2004; Pe'er et al. 2006; Ioka et al. 2007), a firm observational confirmation of the existence of an expected pair annihilation line in the observed GRB spectra was so far lacking. This fact can partially be explained as that the blue-shifted line is expected to be detected in the hundred's of MeVs (the Fermi-LAT) range, in which the detector's sensitivity is poorer than at lower energy bands. In addition, due to relativistic motion, this line may be smeared if the Lorentz factor in different jet regions is somewhat different. Nonetheless, the lack of detection of this line seem to contradict with theoretical expectations.

This situation has changed recently with the observation of GRB221009A, which became known as the 'brightest-of-all-times' (BOAT) GRB. This extremely bright burst had a reported fluence of $F \sim 0.2$ erg/cm² (An et al. 2023; Frederiks et al. 2023; Lesage et al. 2023; Burns et al. 2023). At redshift $z = 0.151$ this implies a record-breaking isotropic energy of $E_{iso} \sim 1.5 \times 10^{55}$ erg as detected by GECAM-C (An et al. 2023), as well as a luminosity exceeding 10^{54} erg/s, which is also among the highest known.

This GRB was so bright that the Fermi-GBM detector was saturated in between 219-277 s from the burst trigger. In addition to being so bright, this burst had several other unique features. Starting at ~ 230 s from the trigger,

extensive TeV emission was detected, with more than 5000 photons detected above TeV (LHAASO Collaboration et al. 2023) and the most energetic photon having an energy as high as 13 TeV (Cao et al. 2023). The TeV emission first rose until ~ 242 s, and then the flux decayed with time roughly as t^{-1} . Furthermore, this burst showed a clear narrow emission line at energy of ~ 10 MeV, separated, in both flux, energy as well as temporal behaviour from the peak of the flux which was at the 100's of keV regime. This line was first identified immediately after the saturation end time (at ~ 280 s), and detected for tens of seconds (Edvige Ravasio et al. 2023; Zhang et al. 2024b). Its energy was observed to decay in time, roughly as $\nu_{line}(t) \propto (t - 226 \text{ s})^{-1}$. Both Edvige Ravasio et al. (2023) and recently Zhang et al. (2024c) have interpreted the line feature as due to high-latitude pair annihilation line emission. However, they did not study the detailed physical conditions to justify that a pair annihilation line with such a luminosity can be realized in this burst.

Here, we explore the consequences of this observation. We focus on understanding the physical conditions that enable the creation of this line, as well as its uniqueness, namely why it has not been detected until recently. As we show below, a relatively narrow range of parameters is required for this line to be detected. We convincingly show that the observed signal decay is indeed due to high latitude emission, and we explore the consequences of this on the jet structure.

2. KEY OBSERVATIONS AND BASIC MODEL ASSUMPTIONS

The observed hard X-ray lightcurve of GRB22109A is very long, lasting for several hundreds of seconds. It is variable, with variability time of a few seconds, and show multiple peaks. The highest peak occurs at ~ 244 s after the GRB trigger. In fact, this peak was so bright that the Fermi-GBM detector was saturated in between the time interval 219-277 s (Edvige Ravasio et al. 2023). The physical origin of this peak is uncertain. In particular, the radius in which energy is dissipated is unknown. However, the fact that the observed spectra is broad, and extends to high energies suggests that the energy dissipation that produces this peak occurs above the photosphere. A likely possibility is that a narrow Poynting flux dominated jet dissipate energy at an emission radius beyond 10^{16} cm (see Zhang et al. (2024a) for arguments).

After the saturation of the GBM detector, clear evidence for emission line emerges. The line energy is in the range of ~ 10 MeV, and decays with time very close to $h\nu_{line}(t) \propto (t - 226 \text{ s})^{-1}$ (see Figure 1). The decay of the flux varies considerably, but may be consistent with a t^{-2} law (see Figure 2). These scaling laws are well consistent with the prediction of high-latitude emission (e.g. Kumar & Panaitescu 2000; Zhang et al. 2009; Zhang 2018).

As a figure of merit, the line luminosity is $L_{line}^{ob.} \approx 10^{50}$ erg/s. It is related to the comoving frame luminosity by $L_{line}^{ob.} = D^2 L'$, where D is the Doppler boost factor (see below). Here and below, we use primes to describe quantities measured in the comoving frame. An underlying assumption of this work is that this observed line is due to pair annihilation. This assumption implies that the rate of pair annihilation must be

$$\dot{N}'^{\pm} = \frac{L'}{2m_e c^2} = \frac{6 \times 10^{55}}{D^2} \text{ s}^{-1}. \quad (1)$$

For simplicity, we assume that the energy dissipation that produces the flux peak at 226 s occurs at a single radius, r , which is the radius when the prompt emission abruptly stops. To estimate this radius, we use the characteristic observed lightcurve variability time scale, $\Delta t \approx 10$ s. This gives

$$r \simeq \Gamma^2 c \Delta t^{ob.} = 1.08 \times 10^{17} \left(\frac{\Gamma}{600} \right)^2 \Delta t_1 \text{ cm}. \quad (2)$$

Here and below, we estimate a fiducial value to the Lorentz factor of $\Gamma = 600$ (Zhang et al. 2024a) for the calculation. In section 4 below, we compare the results with the data, to constrain the value of the Lorentz factor. We further use the standard notation $Q_x \equiv Q/10^x$ in cgs units. Note that this calculation takes into account both the radial and side spreading of the expanding plasma shell.

As the observed spectrum is flat, the flux of energetic photons in the plasma is high. As a result, a large number of pairs are produced. The produced pairs rapidly cool, mainly radiatively, as well as adiabatically. The cold pairs annihilate, producing the observed line. The observed line energy drops with time due to the decrease of the Doppler factor of high latitude emission.

Using the observed (total) burst luminosity $\sim 10^{54}$ erg s^{-1} , one can estimate the photospheric radius to be at

$$r_{ph} = \frac{L\sigma_T}{8\pi m_p c^3 \Gamma^3} = \frac{5.8 \times 10^{20}}{\Gamma^3} L_{54} \text{ cm}. \quad (3)$$

Thus, for jet Lorentz factor of a few hundreds, the assumed radius of pair emission line is much greater than the photosphere. However, this results strongly depends on the value of the jet Lorentz factor, Γ .

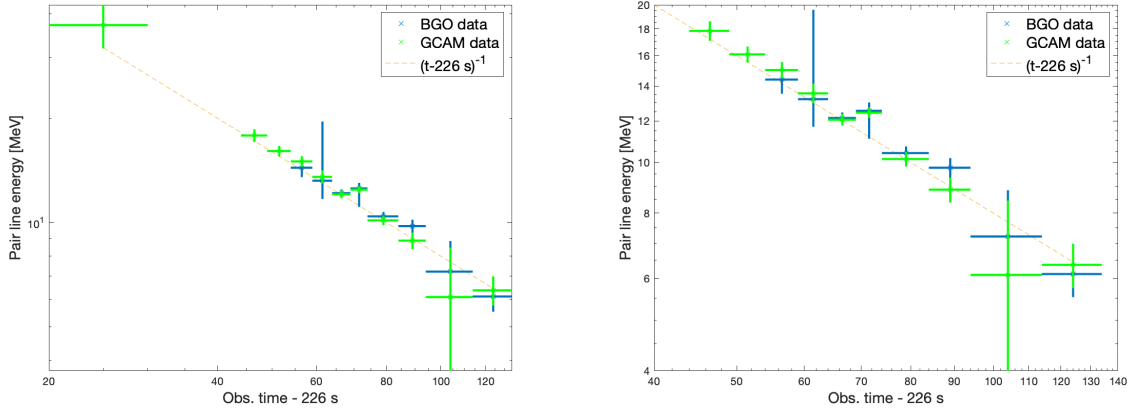


Figure 1. Temporal evolution of the line energy. Left: the full data set; Right: the zoom-in version. Figure made from data taken from the tables given in [Edvige Ravasio et al. \(2023\)](#) and [Zhang et al. \(2024b\)](#).

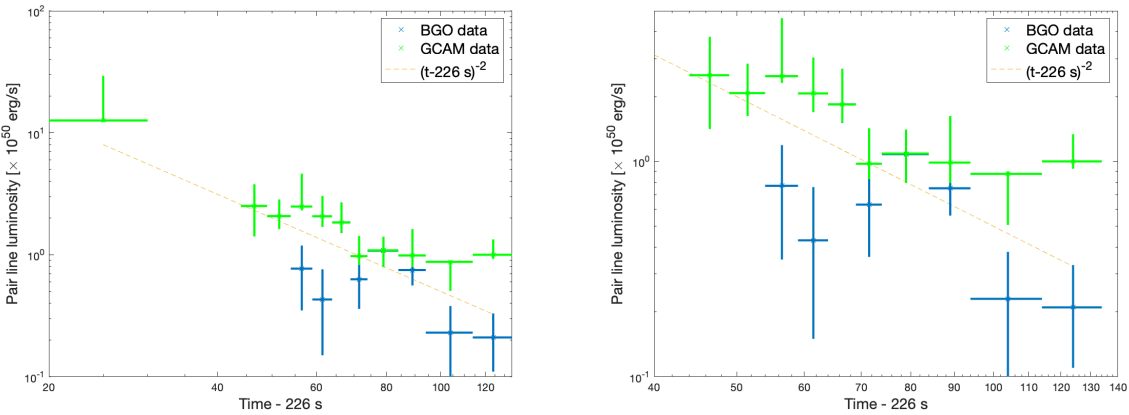


Figure 2. Temporal evolution of the line luminosity. Left: the full data set; Right: the zoom-in version. Figure made from data taken from the tables given [Edvige Ravasio et al. \(2023\)](#) and [Zhang et al. \(2024b\)](#).

3. THEORETICAL EXPECTATION OF THE PAIR ANNIHILATION RATE

The line luminosity is due to annihilation of pairs. In order to estimate the expected luminosity, one needs to calculate the rate of pair annihilation. Here we calculate the theoretical expectation of this rate under various plausible plasma conditions.

3.1. Pair production rate

The pair annihilation rate depends on the density of pairs inside the plasma. As pairs are both produced and annihilated, their density is set by the balance between these two processes. Thus, we first calculate the rate of pair production inside the plasma, from which one can deduce the pair density.

Calculation of the pair production rate is done by estimating the density of photons inside the plasma that are energetic enough to produce pairs. The comoving number density of photons having energies exceeding $\epsilon' \geq Am_e c^2$ is calculated assuming an approximately flat spectra ($\nu F_\nu \propto \nu^0$), which gives an average photon energy $\langle \epsilon' \rangle \approx Am_e c^2$. Here, $A \geq 1$ is an uncertainty factor, which takes into account deviation from a flat spectrum, variation of the cross

section with energy, etc. Its value could be much greater than unity but could be of order of unity, depending on the physical parameters (see more discussion below). For a flat spectrum (which is suggested by both Fermi and GECAM spectral data), the number density of photons in the plasma is therefore

$$n'_\gamma(\epsilon' = Am_e c^2) = \frac{L}{4\pi Am_e c^2 \Gamma^2 c r^2} = \frac{7.7 \times 10^8}{A} L_{54} \Delta t_1^{-2} \left(\frac{\Gamma}{600}\right)^{-6} \text{ cm}^{-3}. \quad (4)$$

The energetic photons interact with low energy photons to produce electron-positron pairs. For a photon with (comoving) energy $Am_e c^2$, the cross section for pair production is maximal for producing a pair with a photon of (comoving) energy $\epsilon' \approx A^{-1} m_e c^2$, and is equal to $\approx \sigma_T$. The typical (comoving) timescale for producing pairs is therefore

$$(t')^{-1} = n'_\gamma(\epsilon') c \sigma_T = \frac{L \sigma_T}{4\pi A^{-1} m_e c^2 \Gamma^2 r^2} = 1.5 \times 10^{-5} A L_{54} \Delta t_1^{-2} \left(\frac{\Gamma}{600}\right)^{-6} \text{ s}^{-1}, \quad (5)$$

or $t' = 6.5 \times 10^4$ s. This value should be compared to the comoving (dynamical) time, $t'_{dyn} = r/\Gamma c = \Gamma \Delta t = 6 \times 10^3 (\Gamma/600) \Delta t_1$ s. The fact that $t' \gg t'_{dyn}$ (for the fiducial parameter values chosen) implies that for these parameter values, only a small fraction of the photons will produce pairs within the available (dynamical) time.

The comoving width of the expanding plasma is $\Delta r' = r/\Gamma$. The optical depth for producing pairs is thus

$$\tau_{\gamma\gamma} = \Delta r' n'_\gamma(\epsilon') \sigma_T = \frac{L \sigma_T}{4\pi A^{-1} m_e c^3 \Gamma^3 r} = 0.092 A L_{54} \Delta t_1^{-1} \left(\frac{\Gamma}{600}\right)^{-5}. \quad (6)$$

Given the high uncertainty in the value of the jet Lorentz factor and the very strong dependence of the optical depth on its unknown value, there is a large uncertainty in the value of the optical depth, $\tau_{\gamma\gamma}$. Since a qualitatively different result is expected for high ($\tau_{\gamma\gamma} > 1$) and low ($\tau_{\gamma\gamma} < 1$) optical depths, we split the calculations into these two regimes: low optical depth and high optical depth for pair production.

3.2. Low optical depth for pair production

For optical depth $\tau_{\gamma\gamma} < 1$, the intensity drops as $I(\tau_{\gamma\gamma}) \simeq I_0(1 - \tau_{\gamma\gamma})$. This means that only a fraction $\tau_{\gamma\gamma}$ of the photons interact to produce pairs before escaping the plasma. In this regime, no sharp cutoff in the high energy spectra that results from high energy photon annihilation is expected. Rather, some gradual decay in the high energy spectra is predicted. We therefore expect in this regime that the value of the uncertainty parameter A will not be too far from unity.

The rate of pair production by a single photon (number of pairs produced per second) is given by $n'_\gamma(\epsilon') c \sigma_T$. Therefore, the density of the pairs produced inside the plasma per unit time is given by

$$\begin{aligned} \dot{n}'_{e\pm} &= n'_\gamma(\epsilon') n'_\gamma(\epsilon') c \sigma_T \\ &= \frac{L^2}{(4\pi A^{-1} m_e c^2 \Gamma^2 c r^2)^2} c \sigma_T = 1.2 \times 10^4 A^2 L_{54}^2 \Delta t_1^{-4} \left(\frac{\Gamma}{600}\right)^{-12} \text{ cm}^{-3} \text{ s}^{-1}, \end{aligned} \quad (7)$$

which is given in units of number per unit volume per unit time. Note the extreme dependence on the values of the parameters, especially the Lorentz factor, Γ .

Assuming that this rate is constant during the dynamical time, $t'_{dyn} = r/\Gamma c$, the density of pairs inside the plasma at the end of the dynamical time is given by

$$n'_{e\pm} = \frac{A^2 L^2 \sigma_T}{(4\pi)^2 (m_e c^2)^2 \Gamma^5 c^2 r^3}. \quad (8)$$

3.2.1. Density of pairs inside the plasma: low optical depth

We assume that the pairs that are produced rapidly cool, reaching typical velocity $v < c$. In this case, the cross section for pair annihilation is $v \sigma_{ann} \simeq c \sigma_T$. The optical depth for pair annihilation is therefore

$$\tau_{e\pm} = \Delta r \sigma_T n'_{e\pm} = \frac{L^2 \sigma_T^2}{(4\pi)^2 (m_e c^2)^2 \Gamma^6 c^2 r^2} = 8.5 \times 10^{-3} A^2 L_{54}^2 \Delta t_1^{-2} \left(\frac{\Gamma}{600}\right)^{-10}, \quad (9)$$

where $\Delta r = r/\Gamma$ was used. This optical depth must be smaller than unity, since $n'_{e\pm} < n'_\gamma$ (this is indeed seen in the equation). Therefore, the rate of annihilation is

$$\dot{n}'_{ann} = (n'_{e\pm})^2 c \sigma_T. \quad (10)$$

We may therefore write the rate equation for the time evolution of pair density inside the plasma:

$$\dot{n}'_{e\pm} = (n'_\gamma)^2 c\sigma_T - (n'_{e\pm})^2 c\sigma_T \equiv C_1 - C_2(n'_{e\pm})^2 \quad (11)$$

(where C_1 and C_2 are constants). The solution to this equation is

$$n'_{e\pm} = n'_\gamma \tanh [(n'_\gamma c\sigma_T)t]. \quad (12)$$

Here, $n'_\gamma = \sqrt{n'_\gamma(\epsilon)n'_\gamma(\epsilon')}$.

This means that in a steady state,

$$n'_{e\pm} \xrightarrow{t \rightarrow \infty} n'_\gamma = 7.7 \times 10^8 A L_{54} \Delta t_1^{-2} \left(\frac{\Gamma}{600}\right)^{-6} \text{ cm}^{-3}, \quad (13)$$

and that the characteristic timescale for approaching this solution is

$$t'_{ss} = \frac{1}{n'_\gamma c\sigma_T} = \frac{4\pi A^{-1} m_e c^2 \Gamma^2 r^2}{L\sigma_T} = 6.5 \times 10^4 A^{-1} L_{54}^{-1} \Delta t_1^2 \left(\frac{\Gamma}{600}\right)^6 \text{ s}. \quad (14)$$

(Note again that all times are measured in the comoving frame). This time should be compared to the (comoving) dynamical time, $t'_{dyn} = r/\Gamma c = 6 \times 10^3 (\Gamma/600)\Delta t_1$ s. One thus concludes: (i) that the time to reach steady state is about an order of magnitude longer than the available time; and (ii) this time depends on Γ . The condition for $t'_{ss} > t'_{dyn}$ is translated into

$$\Gamma > 370 A^{1/5} L_{54}^{1/5} \Delta t_1^{-1/5}. \quad (15)$$

For lower values of Γ , the density of pairs inside the plasma approaches the asymptotic value given in Equation 13 (with an inverse dependence on Γ !). For a larger Lorentz factor, a steady state is not reached.

We proceed by assuming that $t'_{ss} \gg t'_{dyn}$. In this case, one can approximate $\tanh(x) \approx x$, which is valid for $x \ll 1$. Equation 12 then gives the comoving pair density inside the plasma,

$$\begin{aligned} n'_{e\pm}(t') &\approx n'_\gamma (n'_\gamma c\sigma_T)t' = (n'_\gamma)^2 c\sigma_T t' \\ &= \frac{L^2 \sigma_T}{(4\pi)^2 A^{-1} (m_e c^2)^2 \Gamma^4 c r^4} t' = 1.18 \times 10^4 t' A L_{54}^2 \Delta t_1^{-4} \left(\frac{\Gamma}{600}\right)^{-12} \text{ cm}^{-3}. \end{aligned} \quad (16)$$

Note the dependence on the uncertain factor of A is linear.

We may now calculate the rate of annihilation, namely the total number of photons in the emission line that are emitted per unit comoving time (second) from the entire comoving volume,

$$\dot{N}'_{ann} = \dot{n}'_{ann} V' = (n'_{e\pm})^2 c\sigma_T V' \quad (17)$$

(see Equation 10). Here, $V' = 4\pi r^2 c t_{dyn} = 2.6 \times 10^{49} (\Gamma/600)^5 \Delta t_1^3 \text{ cm}^3$ is the comoving volume¹. Putting numbers, one finds:

$$\dot{N}'_{ann} = \frac{L^4 \sigma_T^3}{(4\pi)^3 A^{-2} (m_e c^2)^4 \Gamma^9 c r^5} t'^2 = 7.4 \times 10^{43} t'^2 A^2 L_{54}^4 \Delta t_1^{-5} \left(\frac{\Gamma}{600}\right)^{-19} \text{ s}^{-1}. \quad (18)$$

At $t' = t'_{dyn}$, this reads

$$\dot{N}'_{ann}(t'_{dyn}) = \frac{L^4 \sigma_T^3}{(4\pi)^3 A^{-2} (m_e c^2)^4 \Gamma^{11} c^3 r^3} = 2.7 \times 10^{51} A^2 L_{54}^4 \Delta t_1^{-3} \left(\frac{\Gamma}{600}\right)^{-17} \text{ s}^{-1}. \quad (19)$$

One therefore finds a huge dependence of the pair annihilation rate on the value of the Lorentz factor, Γ . This dependence enables a very wide range of values to be achieved. However, this result holds only as long as the condition in Equation 15 is met, otherwise the optical depth becomes larger than unity, and the parametric dependence becomes different.

It is easy to show that the condition $t'_{ss} > t'_{dyn}$ is equivalent to the condition $\tau_{\gamma\gamma} < 1$. Thus, if the conditions are such that $t'_{ss} < t'_{dyn}$, then $\tau_{\gamma\gamma} > 1$, and one needs to consider the regime of high optical depth, discussed below.

¹ We note that we assume here a constant comoving volume. The error introduced by this assumption is of the order unity.

3.3. High optical depth for pair production

We here explore the other regime, in which the optical depth for pair production, $\tau_{\gamma\gamma} > 1$ (see Equation 6). The condition $\tau_{\gamma\gamma} > 1$ is equivalent to the condition that the comoving time for producing pairs (Equation 5) is smaller than the dynamical time, i.e.,

$$\tau_{\gamma\gamma} > 1 \leftrightarrow t' < t'_{dyn}.$$

Therefore, in this regime, production of pairs occurs on a timescale shorter than the dynamical time. The pair production rate can therefore be estimated as the rate in which energy is produced in photons having energies $\epsilon'_{ph} \geq Am_e c^2$. This rate (per unit volume) is simply

$$\dot{n}'_{e\pm} \approx \frac{L}{(4\pi r^2 \Gamma^2 c)} \frac{1}{Am_e c^2 t'_{dyn}}. \quad (20)$$

The produced pairs rapidly cool. At low energies, the cross section for pair annihilation is also $\sim \sigma_T$. Therefore, the rate of pair annihilation is $\dot{n}'_{ann} \sim n'_{e\pm}{}^2 c \sigma_T$. For large optical depth $\tau_{\gamma\gamma} \gg 1$, there is a balance between pair production and pair annihilation rates, namely $\dot{n}'_{e\pm} = \dot{n}'_{ann}$, giving

$$n'_{e\pm}{}^2 = \frac{L}{(4\pi r^2 \Gamma^2 Am_e c^3 t'_{dyn})} \frac{1}{c \sigma_T} = \frac{L \sigma_T t'_{dyn}}{(4\pi r^2 \Gamma^2 Am_e c^2)} \left(\frac{1}{c \sigma_T t'_{dyn}} \right)^2 = \frac{\tau_{\gamma\gamma} A^2}{(c \sigma_T t'_{dyn})^2}, \quad (21)$$

where we made use of $r \sim \Gamma c t'_{dyn}$.

One therefore finds that in this regime of high optical depth to pair production, the number density of pairs inside the plasma is expected to be

$$n'_{e\pm} \sim \frac{\tau_{\gamma\gamma}^{1/2} A}{c \sigma_T t'_{dyn}} = 2.5 \times 10^9 A^{3/2} L_{54}^{1/2} \Delta t_1^{-3/2} \left(\frac{\Gamma}{600} \right)^{-7/2} \text{ cm}^{-3}. \quad (22)$$

This result further implies that the optical depth to pair annihilation is

$$\tau_{e\pm} = \Delta r n'_{e\pm} \sigma_T = \tau_{\gamma\gamma}^{1/2} A, \quad (23)$$

namely, at any given radius, $\tau_{\gamma\gamma}$ and $\tau_{e\pm}$ are either both greater or smaller than unity.

The rate of annihilation, namely the total number of photons in the emission line that are emitted per unit comoving time from the entire comoving volume, can now be calculated using equation (20),

$$\begin{aligned} \dot{N}'_{ann} &= \dot{n}'_{ann} V' = \dot{n}'_{e\pm} V' = \frac{L}{(4\pi r^2 \Gamma^2 c)} \frac{1}{Am_e c^2 t'_{dyn}} \times 4\pi r^2 c t'_{dyn} = \frac{L}{\Gamma^2 Am_e c^2} \\ &= 3.4 \times 10^{54} A^{-1} L_{54} \left(\frac{\Gamma}{600} \right)^{-2} \text{ s}^{-1}. \end{aligned} \quad (24)$$

Note that essentially, this result means that the brightness of the line is equal to the rate of energy loss from high energy photons by annihilation.

The rate of pair annihilation, as calculated in Equations (19) and (24) for the low and high optical depth regimes is plotted in Figure 3, for different luminosities, together with the inferred value from the data. In the plot, observed variability time $\Delta t = 10$ s was assumed. Values of $A = 1$ (solid lines) and $A = 8$ (dashed lines) were taken for demonstration. This helps explaining the rareness of this line; see further discussion below.

4. THE DOPPLER BOOST: HIGH LATITUDE EMISSION

The observed line show a clear temporal decay, with peak energy that is well fitted as $\epsilon_{\text{line}} = h\nu_{\text{line}} \propto (t - 226 \text{ s})^{-1}$. This temporal behaviour is typical for emission originating at high-latitude, and is due to the evolving Doppler boost.

The comoving pair annihilation line energy ($\epsilon' = 0.5$ MeV) is Doppler boosted towards the observer: $\epsilon^{ob.} = D\epsilon'$. Here,

$$D = \frac{1}{\Gamma(1 - \beta \cos \theta)},$$

where θ is the angle to the line of sight. Under the simplified hypothesis we use here, all the photons are emitted simultaneously at the same radius, r , but at different angles to the line of sight. Since photons emitted at angle θ are delayed with respect to photons emitted on the line of sight by an observed time

$$\delta t^{ob.} = \frac{r}{c}(1 - \cos \theta) \approx \frac{r}{c} \frac{\theta^2}{2},$$

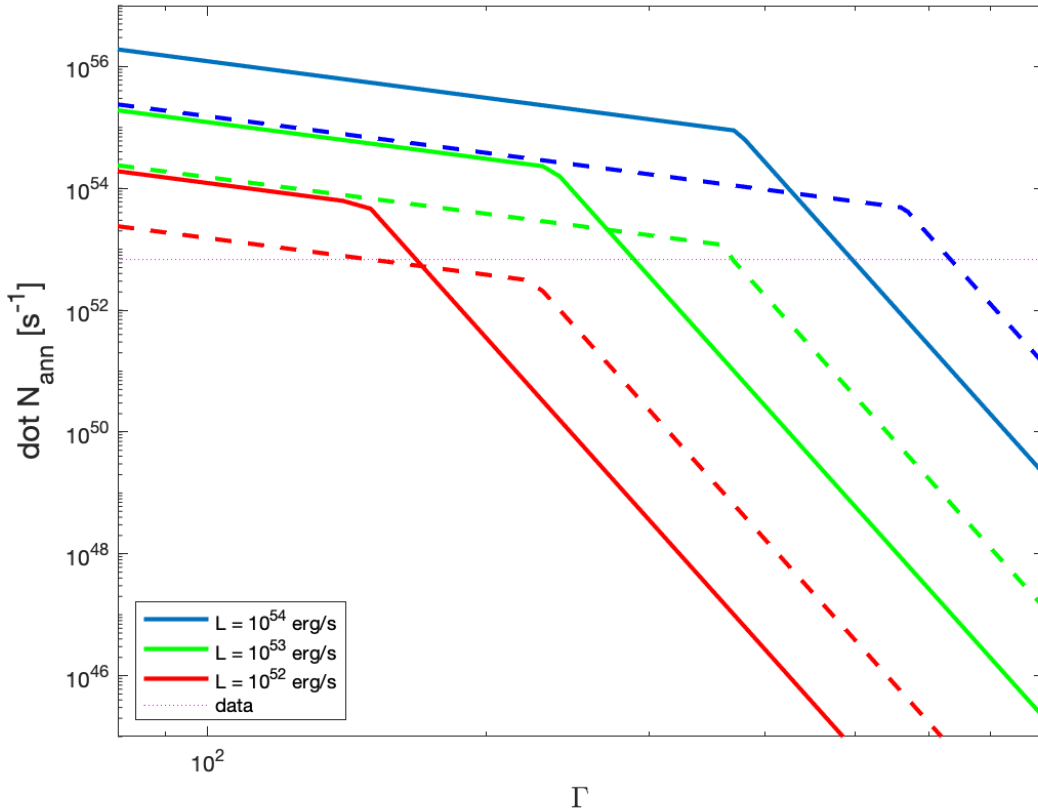


Figure 3. Rate of pair annihilation as a function of the Lorentz factor, Γ , from Equations 19 and 24

At low Γ the system is in the high optical depth to pair production regime, and the rate of annihilation is proportional to Γ^{-2} , while at higher values of Γ (the low optical depth regime), it sharply decays as Γ^{-17} . Solid lines are for $A = 1$, while dashed lines are for $A = 8$ (note that $A = 10$ would result in lines overlap).

one finds the Doppler boost to be

$$\begin{aligned} \theta < \frac{1}{\Gamma} &\rightarrow D \simeq 2\Gamma \propto \delta t^{ob.0}, \\ \theta > \frac{1}{\Gamma} &\rightarrow D \simeq \frac{2}{\Gamma\theta^2} = \frac{r}{\Gamma c \delta t^{ob.}}. \end{aligned} \quad (25)$$

Note that here we use the symbol $\delta t^{ob.}$ to describe the difference between the observed time of the first photon (emitted on the line of sight) and a photon emitted at angle θ to the line of sight, while Δt is used to describe the characteristic observed variability time, from which the emission radius is estimated.

One may now compare this theoretical expectation to the data. About $\delta t^{ob.} \simeq 60$ s after the peak of the flux, the pair annihilation line is at ~ 15 MeV, namely $D \simeq 30$. Using $r = \Gamma^2 c \Delta t$, one finds $r/(\Gamma c) = \Gamma \Delta t = 1800$, or $(\Gamma/600)\Delta t_1 = 0.3$. This result can be combined with the result in Equation (25) (bottom) inside Equation (1), using observed time $\delta t^{ob.} = 60$ s, to write the observational constraint in Equation (1) as a constraint on the rate of pair annihilation at the end of the dynamical time,

$$\dot{N}^{\pm} = \frac{L'}{2m_e c^2} = \frac{L^{ob.}}{2m_e c^2} \left(\frac{\delta t^{ob.}}{\Gamma \Delta t} \right)^2 = 6.8 \times 10^{52} \text{ s}^{-1}. \quad (26)$$

where we took $L^{ob.} = 10^{50}$ erg/s as the luminosity of the line at $\delta t^{ob.} = 60$ from the peak time.

4.1. Low optical depth for pair production

The pair annihilation rate calculated in Equation (26) is to be compared to the theoretical expectation given in Equation (19). Basic algebra reveals that the two results match for $\Gamma = 620 L_{54}^{2/7}$ and $\Delta t = 3.0$ s. Assuming these

value of the Lorentz factor, the dissipation radius is $r = 3.5 \times 10^{16}$ cm, which is much higher than the photospheric radius, at $r_{ph} = 2.4 \times 10^{12}$ cm. The optical depth for pair production is $\tau_{\gamma\gamma} = 0.26 A$, i.e., close to unity, and for pair annihilation it is $\tau_{e\pm} = 0.068$. For these parameters, The time to reach steady state, $t'_{ss} = 7.1 \times 10^3$ s is indeed longer than the dynamical time, $t'_{dyn} = 1.86 \times 10^3$ s (although by a factor of a few only), implying that the approximation we used above is valid.

4.2. High optical depth for pair production

An alternative scenario may be that the emission occurs in region of high optical depth to pair production. In this scenario, the constraint set by the data (Equation 26) is to be compared to the theoretical expectation as given in Equation (24).

The two results match, provided that $(\Gamma/600) = 7 L_{54}^{1/2} A^{-1/2}$. However, too high a value of Γ is unacceptable, as in this case the optical depth for pair production (Equation 6) will be smaller than unity. Using the constraint $(\Gamma/600)\Delta t_1 = 0.3$ inside Equation (6) leads to the constraint

$$0.3AL_{54} > \left(\frac{\Gamma}{600}\right)^4,$$

which, combined with the constraint on the line luminosity above, results in the condition

$$A > 20 L_{54}. \quad (27)$$

This is translated to an expected spectral cutoff at energy

$$\epsilon^{ob.} > 20Dm_e c^2 = 20 \left(\frac{1800 \text{ s}}{t^{ob.}}\right) m_e c^2 = 10 \left(\frac{1800 \text{ s}}{t^{ob.}}\right) \text{ MeV}. \quad (28)$$

this regime is not excluded by existing data, and is therefore valid as well.

5. CONCLUSIONS AND DISCUSSION

5.1. Pair annihilation as a source of the observed line

In this paper, we considered the narrow emission line seen in GRB221009A. We argue that this line originates from e^\pm pair annihilation. We calculated the expected rate of pair annihilation, as a function of the observed GRB parameters, namely the luminosity, a spectral cutoff (A) and variability time, and the unknown jet Lorentz factor. We calculated this rate in the two regimes: low and high optical depths for pair production. The results are presented in Equations (19) and (24), respectively.

When comparing the theoretical expectations to the observed line luminosity, we found that both scenarios are plausible, and both lead to high Lorentz factor, of ~ 600 . The reason why such two different scenarios can provide acceptable explanations is the uncertainty in the cutoff energy, $Am_e c^2$. Therefore, observational discrimination between the two scenarios is possible, by detecting a spectral cutoff (A). For the available data of GRB221009A, this cutoff is expected in the sub-GeV range (Equation 27). This calculation can be trivially generalized to the data of any other source.

5.2. High latitude emission

We explain the observed line energy, as well as the temporal decay of this line as due to emission from high-latitude after the line-of-sight prompt emission is over, i.e., at high angles to the line of sight. This interpretation naturally explains why this line is detected only in the 10 MeV range, rather than the naive expectation of $\Gamma m_e c^2 \sim 300$ MeV range, as would be expected had the emission originated from the line of sight. Indeed, according to our model, at very early times, comparable to $\Delta t \approx 3$ s after the peak (at 226 s), the Doppler boost is expected to be $2\Gamma = 1200$, and the emission line is expected at the sub-GeV range. However, during this time, the detectors are saturated.

Furthermore, this interpretation provides a natural explanation to the temporal decay of the line frequency as $(t - 226 \text{ s})^{-1}$, and its luminosity decay as $(t - 226 \text{ s})^{-2}$, although this is less pronounced by the data. This high latitude interpretation further indicates that the dissipation episode that leads to the emission of this line is instantaneous – it occurs over a short observed period of a few seconds, rather than being continuous. Furthermore, the data clearly

indicates that the energy dissipation episode occurs far above the photosphere, and therefore is not directly related to the on-going events that take place in the central engine during the prompt phase.

Indeed, the high latitude emission model has a firm prediction. Assuming a δ -function emission in time and radius (but that extends over a wide angular range), the observed signal should be constant (time-independent) for a duration of $\Delta t^{ob.} \approx R/(2\Gamma^2 c)$, and after that the flux should drop as Δt^{-2} . This is a universal prediction, which is independent on the origin of the emission, provided it occurs at a constant radius.

This prediction aligns very well with the observed properties of the narrow emission line in GRB221009A. However, this only gives an upper limit on the decay rate of a given signal. Indeed, other parts of the spectra do not follow this behaviour. For example, the peak of the flux seen by Fermi and GECAM is much more variable, and show high peaks at later times, up to 600 s. This indicates that multiple energy dissipation episodes occurred, though none of them provides sufficient energy to produce an observed pair signal.

The TeV flux shows a very different temporal behaviour. While it starts its rise at the same time, 226 s from the trigger, it rises for ≈ 20 s, before decaying as $F_{TeV} \propto t^{-1.1}$, which is much shallower than the limit set by the high latitude emission. The shape of lightcurve is consistent with synchrotron self-Compton scattering from the external shock (LHAASO Collaboration et al. 2023). Since the TeV photons are observed, they are not attenuated to produce pairs, likely because the emission radius is larger than the prompt emission radius where $\tau_{\gamma\gamma}$ is much smaller.

5.3. Rarity of this line

The analysis carried here can be used to explain the lack of detection of pair annihilation line in GRBs so far, despite the clear theoretical prediction. One characteristic of this particular GRB (221009A) is its extreme brightness, $L \simeq 10^{54}$ erg/s (Burns et al. 2023). This is about two - three orders of magnitude brighter than the average GRB.

Assume that for less bright GRBs the detectors would not saturate, continuous observations would occur during the dynamical time. Thus, one could approximate the Doppler boost as $D \simeq 2\Gamma$. The observed line luminosity is expected to be

$$L_{line}^{ob.} = D^2 L' = 4\Gamma^2 \times 2m_e c^2 \dot{N}^\pm.$$

The results of Equations (19) and (24) provide the theoretical expectation,

$$L_{line}^{ob.} = \begin{cases} 6.2 \times 10^{51} L_{54}^4 \Delta t_1^{-3} \left(\frac{\Gamma}{600}\right)^{-15} \text{ erg/s} & \text{(low optical depth)} \\ 7.8 \times 10^{54} A^{-1} L_{54} \text{ erg/s} & \text{(high optical depth).} \end{cases} \quad (29)$$

For typical GRB with luminosity $L \sim 10^{51}$ erg/s, the transition between high and low optical depth occurs at $\Gamma = 90 L_{51}^{1/5} \Delta t_1^{-1/5}$ (see Equation 15). Thus, for typical values of $\Gamma \geq 100$, the valid regime is always the low optical depth regime, where the line luminosity depends on the GRB luminosity to the power 4. In this regime, the theoretical calculations show a huge dependence on the value of Γ , $L_{line}^{ob.} \propto \Gamma^{-15}$. This dependence implies that Γ must have a narrow range of values in order for the line to be detected. E.g., for $L = 10^{51}$, $\Gamma > 150$ will produce a too dim emission line.

For brighter GRBs, this constraint is somewhat releases. For example, for $L = 10^{52}$ erg/s, annihilation line from GRBs with Lorentz factor of 200-250 should be within the detected range, at least for a typical time comparable to the variability time, Δt . In such cases, this line is expected in the same energy range as the line seen in GRB221009A. However, for such a moderate luminosity GRB located at a typical cosmological distance, the line would have too few photons to be detected.

5.4. The dissipation radius

One of the most interesting results of our analysis is that the radius in which energy is dissipated to produce the observed line is large, $r_{dis} \sim 10^{16.5}$ cm. This radius is far above the photospheric radius. On the other hand, this radius cannot be associated with the onset of the afterglow phase, as the data indicates that the prompt emission phase lasts much longer.

The origin of the dissipation process at this radius is therefore not entirely clear. Due to the very large amount of energy released in this radius, We find internal shocks to be a less appealing scenario, as only the differential energy can be released, and as a result the efficiency of energy conversion is very low, typically a few %. The two alternative options are therefore either dissipation of a large amount of magnetic energy (e.g., Zhang & Yan 2011; Zhang et al. 2024a), or alternatively, an abrupt change in the external conditions. As was shown recently (Pe'er & Ryde 2024),

this can naturally occur by interaction of the jet with the contact discontinuity that is naturally expected close to the edge of the wind bubble produced by the progenitor stellar wind.

ACKNOWLEDGEMENTS

AP acknowledge the support from the European Union (EU) via ERC consolidator grant 773062 (O.M.J.).

REFERENCES

- An, Z.-H., Antier, S., Bi, X.-Z., et al. 2023, arXiv e-prints, arXiv:2303.01203, doi: [10.48550/arXiv.2303.01203](https://doi.org/10.48550/arXiv.2303.01203)
- Bošnjak, Ž., Barniol Duran, R., & Pe'er, A. 2022, *Galaxies*, 10, 38, doi: [10.3390/galaxies10020038](https://doi.org/10.3390/galaxies10020038)
- Burns, E., Svinkin, D., Fenimore, E., et al. 2023, *ApJL*, 946, L31, doi: [10.3847/2041-8213/acc39c](https://doi.org/10.3847/2041-8213/acc39c)
- Cao, Z., Aharonian, F., An, Q., et al. 2023, *Science Advances*, 9, eadj2778, doi: [10.1126/sciadv.adj2778](https://doi.org/10.1126/sciadv.adj2778)
- Cavallo, G., & Rees, M. J. 1978, *MNRAS*, 183, 359
- Dereli-Bégué, H., Pe'er, A., Ryde, F., et al. 2022, *Nature Communications*, 13, 5611, doi: [10.1038/s41467-022-32881-1](https://doi.org/10.1038/s41467-022-32881-1)
- Drenkhahn, G. 2002, *A&A*, 387, 714, doi: [10.1051/0004-6361:20020390](https://doi.org/10.1051/0004-6361:20020390)
- Drenkhahn, G., & Spruit, H. C. 2002, *A&A*, 391, 1141, doi: [10.1051/0004-6361:20020839](https://doi.org/10.1051/0004-6361:20020839)
- Edvige Rivasio, M., Sharan Salafia, O., Oganessian, G., et al. 2023, arXiv e-prints, arXiv:2303.16223, doi: [10.48550/arXiv.2303.16223](https://doi.org/10.48550/arXiv.2303.16223)
- Frederiks, D., Svinkin, D., Lysenko, A. L., et al. 2023, *ApJL*, 949, L7, doi: [10.3847/2041-8213/acd1eb](https://doi.org/10.3847/2041-8213/acd1eb)
- Ioka, K., Murase, K., Toma, K., Nagasaki, S., & Nakamura, T. 2007, *ApJL*, 670, L77, doi: [10.1086/524405](https://doi.org/10.1086/524405)
- Krolik, J. H., & Pier, E. A. 1991, *ApJ*, 373, 277, doi: [10.1086/170048](https://doi.org/10.1086/170048)
- Kumar, P., & Panaitescu, A. 2000, *ApJL*, 541, L51, doi: [10.1086/312905](https://doi.org/10.1086/312905)
- Kumar, P., & Zhang, B. 2015, *PhR*, 561, 1, doi: [10.1016/j.physrep.2014.09.008](https://doi.org/10.1016/j.physrep.2014.09.008)
- Lesage, S., Veres, P., Briggs, M. S., et al. 2023, *ApJL*, 952, L42, doi: [10.3847/2041-8213/ace5b4](https://doi.org/10.3847/2041-8213/ace5b4)
- LHAASO Collaboration, Cao, Z., Aharonian, F., et al. 2023, *Science*, 380, 1390, doi: [10.1126/science.adg9328](https://doi.org/10.1126/science.adg9328)
- Lithwick, Y., & Sari, R. 2001, *ApJ*, 555, 540, doi: [10.1086/321455](https://doi.org/10.1086/321455)
- Mészáros, P. 2006, *Reports on Progress in Physics*, 69, 2259, doi: [10.1088/0034-4885/69/8/R01](https://doi.org/10.1088/0034-4885/69/8/R01)
- . 2019, *Mem. Soc. Astron. Italiana*, 90, 57, <https://arxiv.org/abs/1904.10488>
- Mészáros, P., & Rees, M. J. 1993, *ApJ*, 405, 278, doi: [10.1086/172360](https://doi.org/10.1086/172360)
- Mészáros, P., & Rees, M. J. 1997, *ApJL*, 482, L29, doi: [10.1086/310692](https://doi.org/10.1086/310692)
- Pe'er, A. 2015, *Advances in Astronomy*, 2015, 907321, doi: [10.1155/2015/907321](https://doi.org/10.1155/2015/907321)
- Pe'er, A., Mészáros, P., & Rees, M. J. 2006, *ApJ*, 642, 995, doi: [10.1086/501424](https://doi.org/10.1086/501424)
- Pe'er, A., & Ryde, F. 2024, arXiv e-prints, arXiv:2406.03841, doi: [10.48550/arXiv.2406.03841](https://doi.org/10.48550/arXiv.2406.03841)
- Pe'er, A., & Waxman, E. 2004, *ApJ*, 613, 448, doi: [10.1086/422989](https://doi.org/10.1086/422989)
- Rees, M. J., & Meszaros, P. 1992, *MNRAS*, 258, 41P
- . 1994, *ApJL*, 430, L93, doi: [10.1086/187446](https://doi.org/10.1086/187446)
- Shemi, A., & Piran, T. 1990, *ApJL*, 365, L55, doi: [10.1086/185887](https://doi.org/10.1086/185887)
- Woods, E., & Loeb, A. 1995, *ApJ*, 453, 583, doi: [10.1086/176421](https://doi.org/10.1086/176421)
- Zhang, B. 2018, *The Physics of Gamma-Ray Bursts*, doi: [10.1017/9781139226530](https://doi.org/10.1017/9781139226530)
- Zhang, B., & Pe'er, A. 2009, *ApJL*, 700, L65, doi: [10.1088/0004-637X/700/2/L65](https://doi.org/10.1088/0004-637X/700/2/L65)
- Zhang, B., Wang, X.-Y., & Zheng, J.-H. 2024a, *Journal of High Energy Astrophysics*, 41, 42, doi: [10.1016/j.jheap.2024.01.002](https://doi.org/10.1016/j.jheap.2024.01.002)
- Zhang, B., & Yan, H. 2011, *ApJ*, 726, 90, doi: [10.1088/0004-637X/726/2/90](https://doi.org/10.1088/0004-637X/726/2/90)
- Zhang, B.-B., Zhang, B., Liang, E.-W., & Wang, X.-Y. 2009, *ApJL*, 690, L10, doi: [10.1088/0004-637X/690/1/L10](https://doi.org/10.1088/0004-637X/690/1/L10)
- Zhang, Y.-Q., Xiong, S.-L., Mao, J.-R., et al. 2024b, *Science China Physics, Mechanics, and Astronomy*, 67, 289511, doi: [10.1007/s11433-023-2381-0](https://doi.org/10.1007/s11433-023-2381-0)
- Zhang, Z., Lin, H., Li, Z., et al. 2024c, arXiv e-prints, arXiv:2405.12977, doi: [10.48550/arXiv.2405.12977](https://doi.org/10.48550/arXiv.2405.12977)